J. Fluid Mech. (2021), *vol*. 923, A3, doi:10.1017/jfm.2021.538

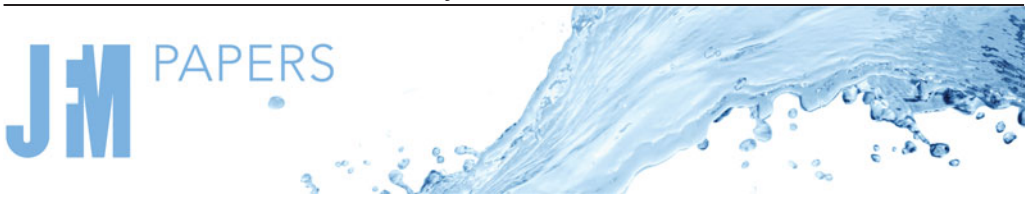

Dynamic and stationary shapes of rotating toroidal drops in viscous linear flows

Sumit Malik[1], **O.M. Lavrenteva**[1] **and A. Nir**[1],†

[1]Department of Chemical Engineering, Technion-Israel Institute of Technology, Haifa 3200003, Israel

(Received 17 September 2020; revised 4 February 2021; accepted 9 June 2021)

Dynamic and stationary axisymmetric deformation of viscous toroidal drops submerged in slow viscous flow are studied numerically. The immiscible ambient fluid is subject to a combination of rotation and extensional/compressional (biextensional) flow. The creeping flow approximation is assumed. The numerical simulations are performed with the help of the boundary integral method. The process under consideration is governed by three dimensionless parameters: the capillary number that characterizes the ratio of viscous and surface tension forces; the Bond number, that characterizes the ratio of centrifugal and surface tension forces; and the ratio of viscosity of the two fluids. Our simulations for the equal viscosity case demonstrated that, depending on the governing parameters, the toroidal drop either collapses, extends indefinitely or it attains a stationary toroidal shape. The latter may be stable or unstable with respect to axisymmetric disturbances. Conditions for the realization of each of the dynamic regimes and stationary states in terms of governing parameters are presented. In particular, stable toroidal shapes result under the combined action of rotation and extensional flow, and were not found under the action of rotation and compressional flow.

Key words: drops, computational methods

1. Introduction

In recent years, the interest in non-trivial forms of fluid particles was stimulated by applications of non-spherical microparticles to have important potential as building blocks for self-assembled materials including clustering of cells, imaging probes for therapy, drug carriers (see, for example, Dean *et al.* (2007), Nurse, Freund & Youssef (2012) and a review by Champion, Katare & Mitragotri (2007)) and more. In particular, toroidal forms are advantageous compared with spherical and spheroidal shapes due to their relatively large surface-to-volume ratio. One of the advanced methods for producing microparticles of complex shapes is solidification of drops deformed by the flow in microfluidic devices.

† Email address for correspondence: avinir@tx.technion.ac.il

Such solidification can be achieved by induction of cross-linking in a polymer drop by ultraviolet radiation (see, for example, Szymusiak *et al.* 2012); see also Shum *et al.* (2010) and Chen *et al.* (2009) for solidification methods involving polymers. Another method of mass production of toroidal forms with sizes in the micrometre to millimetre range via vortex ring freezing was recently demonstrated by An *et al.* (2016) with particular potential for encapsulating DNA segments, cells and bacteria, an application that was also proposed by Chang *et al.* (2015).

Toroidal drops can be obtained in rotating fluid as in Plateau's (1857) experiments and the recent studies of Pairam & Fernández-Nieves (2009) and Pairam *et al.* (2013). Toroidal formation occurs also in the course of free fall of a drop in an immiscible fluid (Baumann *et al.* 1992; Sostarecz & Belmonte 2003), splashing in an immiscible medium (Sharma *et al.* (2012); see figure 1*c*) or by the impact of a droplet with a superhydrophobic surface (Renardy *et al.* 2003) or by head-on collision of two drops (Menchaca R *et al.* 1996). Other mechanisms are by deformation of the drop in electric fields (Deshmukh & Thaokar 2013; Ghazian, Adamiak & Castle 2013) or in magnetic fields (Texier *et al.* 2013). Of particular attention are swarms of particles that can evolve in a viscous fluid into a toroidal shape (Machu *et al.* 2001*b*,*a*). The unique interest in this case is that, although these swarms have practically zero surface tension, they behave dynamically as 'drops' composed of an immiscible different phase. These phenomena have significance in geophysical flows.

Several experimental and theoretical studies are devoted to the question of stability of toroidal drops. The experiments of Pairam & Fernández-Nieves (2009) demonstrated that a toroidal drop in a quiescent fluid is unstable, and it either shrinks and forms a singly connected drop, or it break up via Rayleigh–Plateau instabilities. The shrinking mode was simulated by Ee *et al.* (2018) making use of axisymmetric boundary integral equations (BIE) and the result was compared with the experimental data of Pairam & Fernández-Nieves (2009), showing an excellent agreement. The algorithm in the current study is a modification of the one used by Ee *et al.* (2018). Development of non-axisymmetric three-dimensional shape disturbances was simulated by Mehrabian & Feng (2013) using finite elements on an unstructured and adaptively generated grid. Fragkopoulos & Fernández-Nieves (2017) presented an experimental study of the dynamics of a charged toroidal drop, that results in cross-sections similar in shapes to those shown in this work. It was demonstrated that charging can qualitatively change the behaviour. In some cases it suppressed the shrinking instability, caused the droplet to expand and led to disintegration into small droplets due to Rayleigh–Plateau instabilities.

Several recent papers address theoretically the existence of rotating fluid tori with a deforming free surface (see, for example, Hynd & MacCuan (2006), Nurse, Coriell & McFadden (2015) and the literature cited therein). These analyses are focused on flows in which inertia is the dominant component and viscous forces are neglected. Such tori are typically observed in low viscosity liquids (e.g. by dolphins in water) or in the atmosphere (e.g. by people who smoke). However, the recent and more intensive interest in producing and sustaining toroidal shapes, as for medical purposes mentioned above, is focused on viscous regimes and on toroidal drops with sizes of the order of microns and even less. Hence, recent theoretical efforts are directed toward analyses in which viscous forces are typically dominant, as is addressed below.

The existence of toroidal shapes for drops in a viscous domain was reported as a result of deformation of drops settling in a quiescent fluid, as a consequence of an interfacial instability induced by a finite surface perturbation (Kojima, Hinch & Acrivos 1984). They also studied the dynamics of a highly expanded slender toroidal drop, in their nomenclature a torus having radius, b, much larger than the cross-section dimension, ϵb,

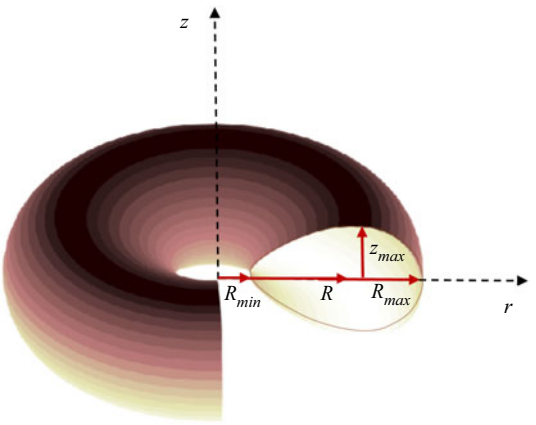

Figure 1. A toroidal drop with $R = (R_{min} + R_{max})/2$.

with $\epsilon \ll 1$, making use of matched asymptotic expansion techniques, and showed that such a settling drop can expand only if small effects of inertia are incorporated into the analysis. On the other hand, the numerical simulations of Machu *et al.* (2001*b*) and Machu *et al.* (2001*a*) demonstrated that the non-slender torus can expand also in quasi-static Stokes flow. In practice, obtaining toroidal shapes from a spherical drop via sedimentation is demonstrated vividly by several works (e.g. Baumann *et al.* 1992; Sostarecz & Belmonte 2003; Szymusiak *et al.* 2012). Fontelos, Garcia-Garrido & Kindelán (2011) used a boundary integral approach to simulate the evolution and breakup of a viscous rotating drop under the quasi-stationary approximation. The toroidal stationary shape of a rotating drop was found among various families of axisymmetric and asymmetric forms. Zabarankin, Lavrenteva & Nir (2015) and Ee *et al.* (2018) numerically analysed the deformation of an immiscible toroidal drop embedded in axisymmetric compressional (biextensional) Stokes flow making use of the boundary integral formulation. These studies confirmed the prediction obtained earlier that a spherical drop, experiencing such viscous forcing, becomes flat, eventually loses stability and becomes toroidal (Zabarankin *et al.* 2013). Numerical simulations of the quasi-stationary dynamics performed revealed that, when the viscous forces, proportional to the intensity of the flow, are relatively weak compared with the surface tension (the ratio of these forces is characterized by the capillary number, *Ca*), three different scenarios of drop evolution are possible: indefinite expansion of the liquid torus; contraction and collapse to the centre; and a stationary toroidal shape. Here, and in what follows, torus expansion or collapse refers to increase or decrease in its radial dimensions, respectively. These dimensions are defined below in figure 1. When the intensity of the flow is low, the stationary shapes are shown to be close to circular tori. Once the outer flow strengthens, the cross-section of the stationary torus assumes first an elliptic and then an egg-like shape. For capillary numbers greater than a critical value, toroidal stationary shapes were not found.

A main common finding in the general case is that all toroidal stationary states of a drop under rotating or biextensional outer flow are unstable and that any infinitesimal axisymmetric perturbation will cause a collapse or an infinite expansion of the torus. Indeed, the dynamics will vary between cases, but no stable shapes are predicted.

In the present work we study the evolution and stationary axisymmetric deformation of a toroidal viscous drop submerged in viscous fluid subject to a combination of rotation and extensional or compressional (i.e. biextensional) flow. We follow the work of Malik,

Lavrenteva & Nir (2020), who investigated the deformation of a spherical drop embedded in the combination of these viscous flows, where the joint action of the two types of flow are presented in the normal component of the stress boundary condition, expressed in terms of capillary and Bond numbers. Malik *et al.* (2020) reported on the boundaries of the domain of parameters in which the drop deformation resulted in stable singly connected bodies. Beyond these boundaries the drop deformation becomes unstable and, in some cases, can result in toroidal shapes. Our present simulations demonstrate that, depending on the governing parameters and the initial conditions, a liquid torus collapses to a singly connected shape, or extends indefinitely, or it attains a stationary toroidal shape. Conditions for the realization of each scenario in terms of governing parameters are presented. In particular, it is demonstrated that under the combined action of rotation and extensional flow multiple toroidal stationary shapes exist, with one of them being stable, at least with respect to axisymmetric perturbations. Note that in the absence of any one of these two components of the outer flow no stable toroidal shapes were found. It is noted that the paper does not include a stability analysis, and it is assumed that onset of loss of stability toward collapse or extension preserves an axially symmetric shape. Nevertheless, it can be expected that both stationary stable and unstable shapes, observed in this study, may be subject to three-dimensional disturbances such as, for example, capillary driven perturbations. A complete stability analysis of such phenomena deserves a separate study.

The paper is organized as follows. In § 2, the problem of the dynamic and stationary deformation of a liquid torus in axisymmetric linear viscous flow is formulated. Section 3 describes the details of the numerical method. In § 4, the problem of toroidal drop deformation in the rotating fluid is revisited and the results are presented in a form convenient to the comparison with the more general case. Section 5 outlines numerical results showing the dynamic evolution of the toroidal drops under the combined action of rotation and extensional or compressional flow, and the conditions in which stationary drops are obtained for the various values of the governing parameters. Stable and unstable stationary toroidal drops are shown and discussed in § 6, and a summary of the multiplicity of toroidal stationary solution branches is presented in the phase plane of parameter space. The existence of this space constitutes the primary objectives of this paper. The relation to the relevant singly connected solution branches is also demonstrated. A short discussion is given in § 7.

2. Mathematical model

Consider a viscous toroidal drop (figure 1) of viscosity μ and constant volume V which is embedded in an unbounded viscous fluid having viscosity equal to that of the drop. We assume that the drop and the external fluid are rotating axisymmetrically with angular velocity ω. The study is conducted in the presence of external flow effects. External flow is a combination of rotation and extensional or compressional (biextensional) flow which, in the absence of the drop, is given by

$$u_i^{\infty} = \pm G_{ij}x_j + \epsilon_{ijk}\omega_j x_k, \tag{2.1}$$

where $G_{11} = G_{22} = G$, $G_{33} = -2G$ and $G_{ij} = 0$ if $i \neq j$. Here G denotes the constant shear rate and $\omega_j = \omega\delta_{j3}$. The positive and negative signs in (2.1) denote compressional and extensional modes of flow, respectively, whereas, in the absence of external flow we have $G = 0$. Let $D^{(1)}$ and $D^{(2)}$ be the domains occupied by the drop and the ambient fluid and $u^{(1)}$, $p^{(1)}$ and $u^{(2)}$, $p^{(2)}$ denote the velocity and pressure fields in $D^{(1)}$ and $D^{(2)}$, respectively. Assuming a creeping flow, and ignoring inertia and sedimentation effects, the

velocity and pressure fields satisfy the following Stokes equations, in coordinates rotating at angular velocity ω:

$$-\nabla p^{(i)} + \mu^{(i)} \Delta \boldsymbol{u}^{(i)} - \rho_i \boldsymbol{\omega} \times (\boldsymbol{\omega} \times \boldsymbol{r}) = 0, \quad \text{in } D^{(i)}(t), \tag{2.2}$$

$$\nabla \cdot \boldsymbol{u}^{(i)} = 0, \quad \text{in } D^{(i)}(t), \ i = 1, 2. \tag{2.3}$$

At the drop interface, S, the velocity and stress balance conditions are given by

$$u^{(1)} = u^{(2)} \tag{2.4}$$

and

$$(\tau^{(2)}{}_{ij} - \tau^{(1)}_{ij}) n_j = \gamma \frac{\partial n_j}{\partial x_j} n_i, \tag{2.5}$$

where γ is the constant interfacial tension and $\boldsymbol{n}$ is the unit normal vector pointing outwards of the drop surface. Here $\tau^{(1)}$ and $\tau^{(2)}$ denote the stress tensors inside and outside the drop, given as

$$\tau_{ij} = -p\delta_{ij} + \mu \left(\frac{\partial u_i}{\partial x_j} + \frac{\partial u_j}{\partial x_i} \right). \tag{2.6}$$

Far from the drop, the pressure and velocity approach those of the undisturbed fields $p^{(2)} \to p^{\infty}$ $u^{(2)} \to \boldsymbol{u}^{\infty}$. For a fixed axis of rotation a modified pressure (Fontelos *et al.* 2011) can be written as

$$P^{(i)} = p^{(i)} - \frac{\rho_i \omega^2 r^2}{2}, \tag{2.7}$$

where $\omega = |\boldsymbol{\omega}|$ and r denotes the distance of $\boldsymbol{r}$ from the axis of rotation. Substituting (2.7) into (2.2) results in

$$-\nabla P^{(i)} + \mu^{(i)} \Delta \boldsymbol{u}^{(i)} = 0, \quad \text{in } D^{(i)}(t), \ i = 1, 2 \tag{2.8}$$

with

$$u_i^{\infty} = \pm G_{ij} x_j. \tag{2.9}$$

Note that (2.8) and (2.9) coincide with the form of the equations for the study of a Stokes flow under shearing force. However, the introduction of the rotation mode is hidden in the rotating coordinate system and is expressed explicitly in (2.13).

Introducing the characteristic length and velocity as l and U, respectively, we define non-dimensional variables as

$$\bar{x} = \frac{x}{l}, \quad \bar{\boldsymbol{u}}^{(i)} = \frac{u^{(i)}}{U}, \quad \bar{P}^{(i)} = \frac{lP^{(i)}}{\mu U}, \quad \overline{\rho_i} = \frac{\rho_i}{\rho_1}, \quad \bar{\tau}^{(i)}_{jk} = \frac{l\tau^{(i)}_{jk}}{\mu U}, \tag{2.10a–e}$$

where l is the undisturbed spherical drop radius given by $l = \sqrt[3]{3V/4\pi}$ and U is yet to be defined in §§ 3 and 5. For the sake of brevity, we will omit the overbars from non-dimensional variables in the forthcoming part. Finally, the non-dimensional form of

(2.8), (2.3) and (2.5) can be written as

$$-\nabla P^{(i)} + \Delta \boldsymbol{u}^{(i)} = 0, \quad \text{in } D^{(i)}(t), \tag{2.11}$$

$$\nabla \cdot \boldsymbol{u}^{(i)} = 0, \quad \text{in } D^{(i)}(t)\ i = 1, 2, \tag{2.12}$$

and the modified interfacial stress difference

$$\left(\tau_{ij}^{(2)} - \tau_{ij}^{(1)}\right) \boldsymbol{n}_j = \frac{1}{Ca}\left(\frac{\partial n_j}{\partial x_j} - \frac{Bo}{2} r^2\right) \boldsymbol{n}_i, \quad \text{on } S, \tag{2.13}$$

with Ca being the capillary number and Bo being the Bond number defined by

$$Ca = \frac{\mu U}{\gamma}, \quad Bo = \frac{(\rho_1 - \rho_2)\omega^2 l^3}{\gamma}, \tag{2.14a,b}$$

where $\sqrt{|Bo|}$ gives the dimensionless angular velocity intensity.

3. Solution methodology

The problem of simulating a rotating drop can be studied in the absence or presence of an external flow field. The former case can be simulated by solving ordinary differential equations for the solid body rotation (Aussillous & Quéré 2004; Heine 2006; Fontelos *et al.* 2011; Malik *et al.* 2020). In the presence of external flow more advanced methods of solution such as boundary elements and BIE methods were used by Fontelos *et al.* (2011) and Malik *et al.* (2020). In this paper we have used both mentioned methods as and when required. A short summary is provided below.

3.1. *Method of ordinary differential equations*

In the absence of an external shear flow, the drop has a stationary shape and the entire external medium rotates in solid body rotation. In this case $U = \gamma/\mu$ and, in view of (2.14*a*,*b*), $Ca = 1$. The equilibrium shapes of a drop can be obtained by integrating the following differential equation (Fontelos *et al.* 2011):

$$\kappa = -P + \frac{Bo}{2} r^2, \tag{3.1}$$

where κ denotes the mean curvature of drop surface and P is the modified pressure difference across the drop interface, which is constant. The geometry of a drop is defined with the help of a function $g(r)$, that gives the height of the interface as a function of r, i.e. the distance from the axis of rotation. Under the assumption of axial symmetry, we have

$$\kappa = -\frac{1}{r}\frac{\mathrm{d}}{\mathrm{d}r}\left(\frac{r g_r}{\sqrt{1 + g_r^2}}\right). \tag{3.2}$$

Following Fontelos *et al.* (2011), (3.1) and (3.2) lead to the relation

$$\int_a^{r_{max}} \frac{Bor^5 - 4Pr^3 - (8a + Boa^4 - 4Pa^2)r}{\sqrt{1 - \left(\frac{Bo}{8} r^3 - \frac{P}{2} r - \left(\frac{a + \frac{Bo}{8} a^4 - \frac{P}{2} a^2}{r}\right)\right)^2}} = \frac{16}{3}, \tag{3.3}$$

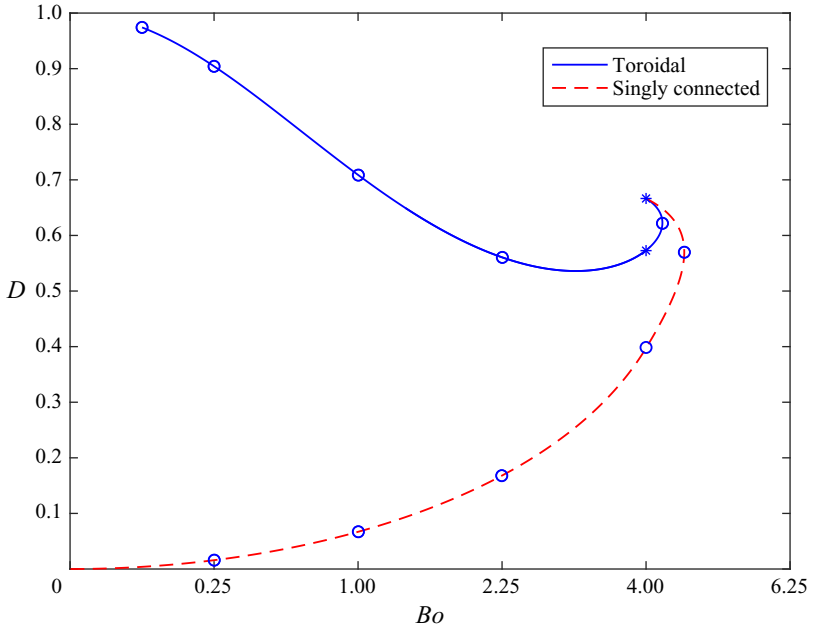

Figure 2. Deformation ($D = (R_{max} - z_{max})/(R_{max} + z_{max})$) of stationary toroidal (blue) and singly connected (red) drops for varying Bo when $G = 0$.

where (see figure 1) r_{max} and a can be obtained from

$$\frac{Bo}{8} r_{max}^3 - \frac{P}{2} r_{max} - \left(\frac{a + \dfrac{Bo}{8} a^4 - \frac{P}{2} a^2}{r_{max}} \right) = 1. \tag{3.4}$$

The solution of (3.3) and (3.4) give the shape of a toroidal drop with $a = r_{min}$. The same formulation leads to a simply connected drop when $a = 0$.

Figure 2 shows the complete pattern of deformation, in the absence of external flow, under which a spherical shaped drop takes the form of toroidal drop after breakup at the critical point. The critical point for the breakup of the drop is obtained when $Bo = 4.0004$ with a deformation factor given by 0.6665. The two starred points are highlighted as they play a special role in the results presented in § 6.

3.2. *Boundary integral method*

The solution via ordinary differential equations is limited to the case in which there is no external flow. In the presence of extensional or compressional effects of external flow, the solution of the Stokes equations (see 2.11), together with boundary conditions (2.4) and (2.13), is obtained by using the boundary integral method. Here, we consider a cylindrical coordinate system (r, ϕ, z) where the z-axis coincides with the axis of rotation. For a given shape of drop and equal viscosities of the drop and the ambient fluid, the solution of the Stokes equations can be written as follows:

$$u_j(\boldsymbol{x}_p) = u_j^{\infty} - \frac{1}{8\pi Ca} \int_S \left(\kappa(\boldsymbol{x}) - \frac{1}{2} Bor^2 \right) n_i(\boldsymbol{x}) J_{ij}(\boldsymbol{x}, \boldsymbol{x}_p) dS(\boldsymbol{x}), \tag{3.5}$$

which consists of a direct evaluation of the velocity from the integral that is comprised of geometrical variables only. Here, $\boldsymbol{x}_p$ denotes the position vector of point p, and

$$J_{ij}(\boldsymbol{x}, \boldsymbol{x}_p) = \frac{\delta_{ij}}{|\boldsymbol{x} - \boldsymbol{x}_p|} + \frac{(x_i - x_{p,i})(x_j - x_{p,j})}{|\boldsymbol{x} - \boldsymbol{x}_p|^3}. \tag{3.6}$$

Here δ_{ij} is the Kronecker delta and $\boldsymbol{u}^{\infty} = \pm(Gl/U)(1, 1, -2)$ in which positive and negative signs represent compressional and extensional flow, respectively. The expressions for the kernels can be found in Pozrikidis (1992).

The stability and stationarity of a drop can be decided by computing its dynamical deformation. A drop is considered to be stationary if the shape remains constant for a relatively long period of time. A stationary drop is said to be stable if after a certain time the drop shape remains unchanged indefinitely, i.e. the deformation factor of drop becomes constant, and the normal velocity component of the surface elements diminishes. In this study, the drop deformation factor for the toroidal drop is defined as (Zabarankin *et al.* 2015)

$$D = \frac{R_{max} - z_{max}}{R_{max} + z_{max}}, \tag{3.7}$$

where R_{max} is the maximum distance of drop interface from the centre of drop at $z = 0$. Also, z_{max} is the maximum distance of the drop interface in the z-direction from the plane $z = 0$ as shown in figure 1. A stationary drop is considered unstable if any small deformation of the shape results in its deviation from stationarity.

Recently, the solution of (3.5) for simply connected shapes has been obtained and discussed by Malik *et al.* (2020). In the present study, we have a doubly connected region, more specifically, a toroidal-like structure for which we employed a similar approach for the solution. As discussed by Zabarankin *et al.* (2015), the simulation of quasi-stationary dynamic deformation of toroidal drop can be made by assuming some initial shape (Rallison & Acrivos 1978). In the current problem, the simulation process is started with a circular cross-section of a toroidal shape having a volume equal to that of a unit sphere. The shape is then allowed to deform with calculated velocity on the boundaries and a possible stable or unstable stationary solution is attained. A general process, applied in the simulation, is as follows.

(i) Consider an initial shape S_t as a torus having a circular cross-section at time $t = 0$.
(ii) Partition S_t to N evenly distributed boundary elements and represent each element by a cubic spline parameterized by the arclength.
(iii) Calculate unit normal vector and curvature in each surface element using cubic splines.
(iv) Evaluate the boundary integral given in (3.5) throughout the surface using Gauss–Legendre quadrature with singularity subtraction (Pozrikidis 1992) and obtain a velocity profile $\boldsymbol{u}$.
(v) Evaluate the norm of the normal component of the surface $\|u_n\|^2 = (1/\int \mathrm{d}S) \int \|u^2\| \,\mathrm{d}S$.
(vi) If $\|u_n\| < \epsilon$, where ϵ is a small tolerance level, we accept this shapes as a stationary state. Otherwise we update the time by $t = t + \Delta t$ and the surface of drop S_t using the rule

$$S_{t+\Delta t} = S_t + \boldsymbol{u}\Delta t \tag{3.8}$$

and go to step (ii) with updated parameters to continue in a similar manner.

For the validation of simulated results we have compared the drop deformation with those of Ee *et al.* (2018), in the case of $Bo = 0$ and equal viscosity of the drop and the ambient fluid with varying Ca values. The calculated results of both codes are in excellent agreement.

4. Stable and stationary axisymmetrically rotating drop in the absence of external shear flow (Fontelos *et al.* (2011) revisited)

In this section we study the stable and unstable stationary rotating drops (singly connected and toroidal), embedded in a rotating frame of reference, in the absence of compressional or extensional external flow, i.e. when $G = 0$. The transformation from singly connected drop to a toroidal drop has always been a case of special interest, hence, a detailed discussion, including the particular case of transformation point $Bo = 4.0004$ is provided in § 6, where a few cases of singly connected drops are compared with relevant toroidal shapes. While following Fontelos *et al.* (2011) our interest somewhat diverges. We are less interested in the influence of the forcing flow on the moment of inertia but, rather, our focus is on the deformation. Furthermore, much of their attention is devoted to drops that possess a very thin film connecting a toroidal rim (termed type-II) while this paper concentrates on toroidal rings. The work of Fontelos *et al.* (2011) is an excellent gateway to concentrate on combining the rotation with an additional shear field, in which case there exist characteristics and special results that are discussed below and are relevant to the more general study discussed in the following sections.

As mentioned in section § 3.1, the drop simulation in the absence of external flow effects is obtained by solving (3.1) and (3.2), which enables us to yield multiple solutions for drop stationarity deformation (Malik *et al.* 2020) with a relatively high accuracy. The multiple solutions include both singly connected and toroidal stationary shapes for varying Bo values. Figure 2 presents the deformation pattern of singly connected and toroidal drops in equilibrium shape when $G = 0$ and $U = \gamma/\mu$. We recognize three distinct regions in the interval $0 < Bo < 4.5497$, having two, three and four different solutions of (3.1) and (3.2) representing different stationary shapes.

In the subregion $0 < Bo < 4.0004$ we identify two solutions. The lower branch is comprised of singly connected bodies, with the shape's deformation changing continuously from a spherical drop at $Bo = 0$ up to an oblate flat drop at $Bo = 4.0$. The upper branch displays a toroidal shape's deformation changing continuously from a torus of infinite extent and vanishing circular cross-section at $Bo = 0$, to an almost collapsed torus with an egg shape cross-section at $Bo = 4.0$. The flat and toroidal drop shapes at $Bo = 4.0$ have deformation factors $D = 0.3974$ and 0.5731, respectively, and are depicted in figure 3(a). The stationary flat oblate shapes in this region of Bo are stable (see Fontelos *et al.* 2011; Malik *et al.* 2020) while the stationary toroidal shapes were suggested by Fontelos *et al.* (2011) to be unstable. Indeed, this assumption is validated in § 6, below, for the more general Bo analysis where the deformation curves are also obtained by solving the BIE, and where infinitesimal perturbations grow indefinitely.

A second region of Bo, where two solutions to the problems (3.1) and (3.2) coexist, is in the interval $4.2312 < Bo < 4.5497$. In this region we observe only singly connected shapes. Here $Bo = 4.5497$ is the turning point, shown in figure 2, and denotes the maximum value of Bo (with $G = 0$) for which stationary shapes exist. At this location $D = 0.5702$, its rate of change with Bo is infinite, and dimples are evident at the axis of symmetry on both sides of the symmetry plane at $z = 0$, with an ever growing negative curvature component as the deformation factor increases toward $D = 0.6480$ at

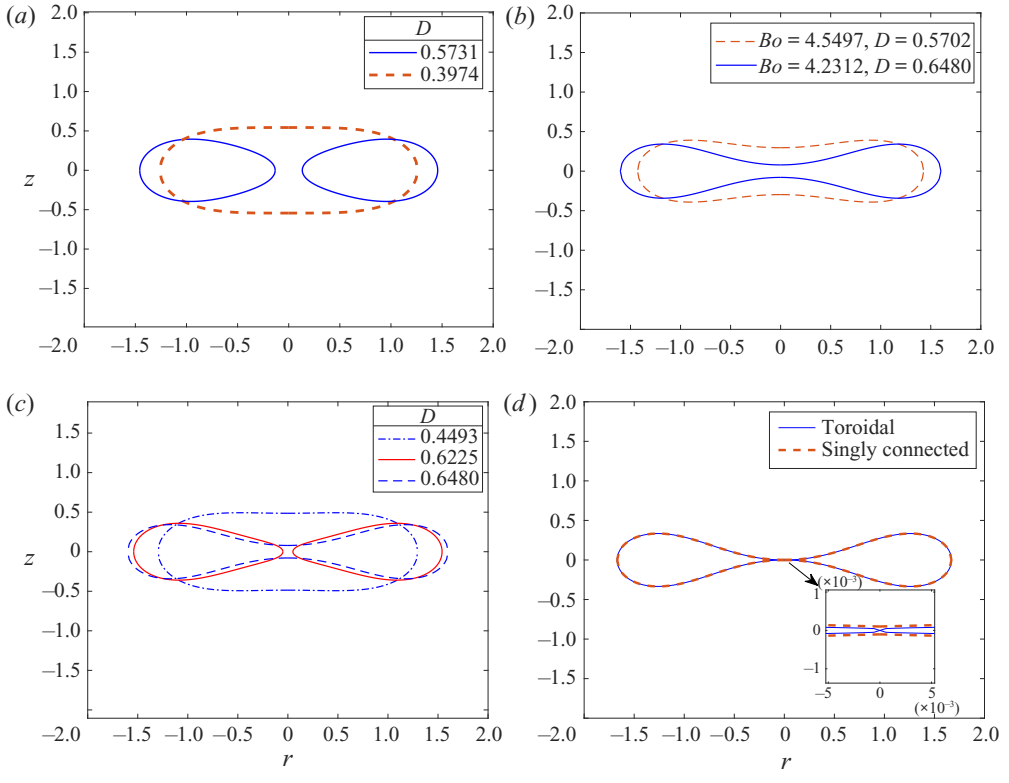

Figure 3. (*a*) Shapes of toroidal and singly connected drop at $Bo = 4$; (*b*) shapes of evolution of dimples in singly connected drop; (*c*) multiple shapes of stationary toroidal and singly connected drops for $Bo = 4.2312$; (*d*) comparison of shapes of toroidal and singly connected drop at critical transition region when $G = 0$.

$Bo = 4.2312$ and beyond. Shapes with evolution of such dimples are shown in figure 3(*b*). Note that all flat shapes below $D = 0.5702$ (where $Bo = 4.5497$) are stable, while flat shapes beyond this D value, are unstable (Malik *et al.* 2020).

We turn next to the region in the intermediate interval $4.0004 < Bo < 4.2312$. The boundaries of this interval represent special points. At $Bo = 4.2312$ we observe (see figure 2) a turning point beyond which no toroidal solutions exist. The deformation factor there is $D = 0.6225$. Thus, at this particular Bo value there are three stationary solutions to (3.1) and (3.2), the limiting toroidal shape and two singly connected shapes, i.e. a stable flat one and an unstable dimpled one. These are shown in figure 3(*c*). The boundary point $Bo = 4.0004$, at which $D = 0.6665$, is a point at which transition from a singly connected shape to a toroidal one occurs. At this point either the evolving dimples in the stationary flat drop reach both sides of the symmetry plane $z = 0$ and a toroidal drop may form or, *vice versa*, a stationary toroidal drop reached its ultimate collapsed shape and converts into a dimpled drop. It is noted that a focus on such transitions should involve thin layer stability analysis integrating hydrodynamic, intermolecular and thermodynamic considerations, and is not in the scope of this manuscript. Nevertheless, the shapes on both 'sides' of the transition point were calculated and are depicted in figure 3(*d*).

As is evident in figure 2 the interval $4.0004 < Bo < 4.2312$ contains four solutions to (3.1) and (3.2). There are two singly connected shapes and two toroidal. The flat

stable shape has a minimum deformation factor while the dimpled unstable one shows a maximum deformation, and the two toroidal deformation values are located in-between.

We close this subsection concluding that, depending on the value of the Bond number, in the absence of an additional external shear, the solution of problem (3.1) and (3.2) results in branches that exhibit several stationary drop deformations with different shapes, some stable and others unstable. Note that our analysis does not contain the toroidal type-II branch discussed by Fontelos *et al.* (2011), i.e. consisting of a zero thickness film connecting a toroidal rim, as it assumes that toroidal type-I shapes, having $R_{min} > 0$, are more likely to be a preferred result of the unstable situation once the dimples touch.

5. Dynamics and evolution of rotating toroidal drops under the action of extensional or compressional flow

In this section we study the dynamics of axisymmetrically rotating drops under the influence of compressional or extensional flow at various Ca for fixed Bo values lying within the range of $[-5, 5]$. The simulation of drop deformation is conducted with the help of the boundary integral method due to the involvement of external flow effects, as explained in § 3.2. The initial drop is considered to be a torus of circular cross-section which is subjected to axisymmetric extensional or compressional viscous flow. The dynamics of the deformation of the rotating torus under the mentioned effects is governed by various forcing: the surface tension which tends to shrink the torus; the drop viscosity that slows down the deformation; the rotation which tries to expand or collapse the torus, depending on the density differences; the external flow. Here, the external flow is one of two types: a compressional flow, which tends to expand the torus; or an extensional flow, which tends to collapse it. Based on these forces the drop dynamics is studied to yield possible stable or unstable stationary shapes. For the sake of clarity, in what follow the non-dimensional velocity is scaled with unit of $U = Gl$ and the results related to extensional flow are presented using negative signs of Ca, whereas the region $Ca > 0$ represents the compressional flow. From the definition of Bo given in (2.14*a*,*b*), when $Bo < 0$, the drop is said to be lighter than ambient fluid and $Bo > 0$ represents a relatively heavier drop.

Figures 4–7 represent the time evolution of various factors defining the dynamic deformation of the drop. In addition to D these include the radial distance to the centre of the torus cross-section, R, and the deformation of the cross-section of the torus, D_{cs}, defined as

$$R = \frac{R_{min} + R_{max}}{2} \quad \text{and} \quad D_{cs} = \frac{R_{max} - R_{min} - 2z_{max}}{R_{max} - R_{min} + 2z_{max}}, \tag{5.1a,b}$$

where R_{min}, R_{max} and z_{max} are presented in figure 1. Note that the superscripts u and s used in figures denote the values of the respective parameters at the unstable stationary and stable stationary states of toroidal drops, respectively, discussed below.

5.1. *Rotating drops in compressional flow*

Figures 4 and 5 show the typical evolution of these parameters for the case of light drops in compressional flow for various values of the initial major radius, $R(0)$. In figure 4, $Bo = -1$ and $Ca = 0.21$, while in figure 5, $Bo = -3$, $Ca = 0.3$. In the presented cases, R, D and D_{cs} initially increase. There exists a critical value of $R(0)$ for which the drop shape parameters do not change for a considerable length of time, which is denoted by R_c. Note that we have calculated R_c to a high degree of accuracy that is needed to identify the

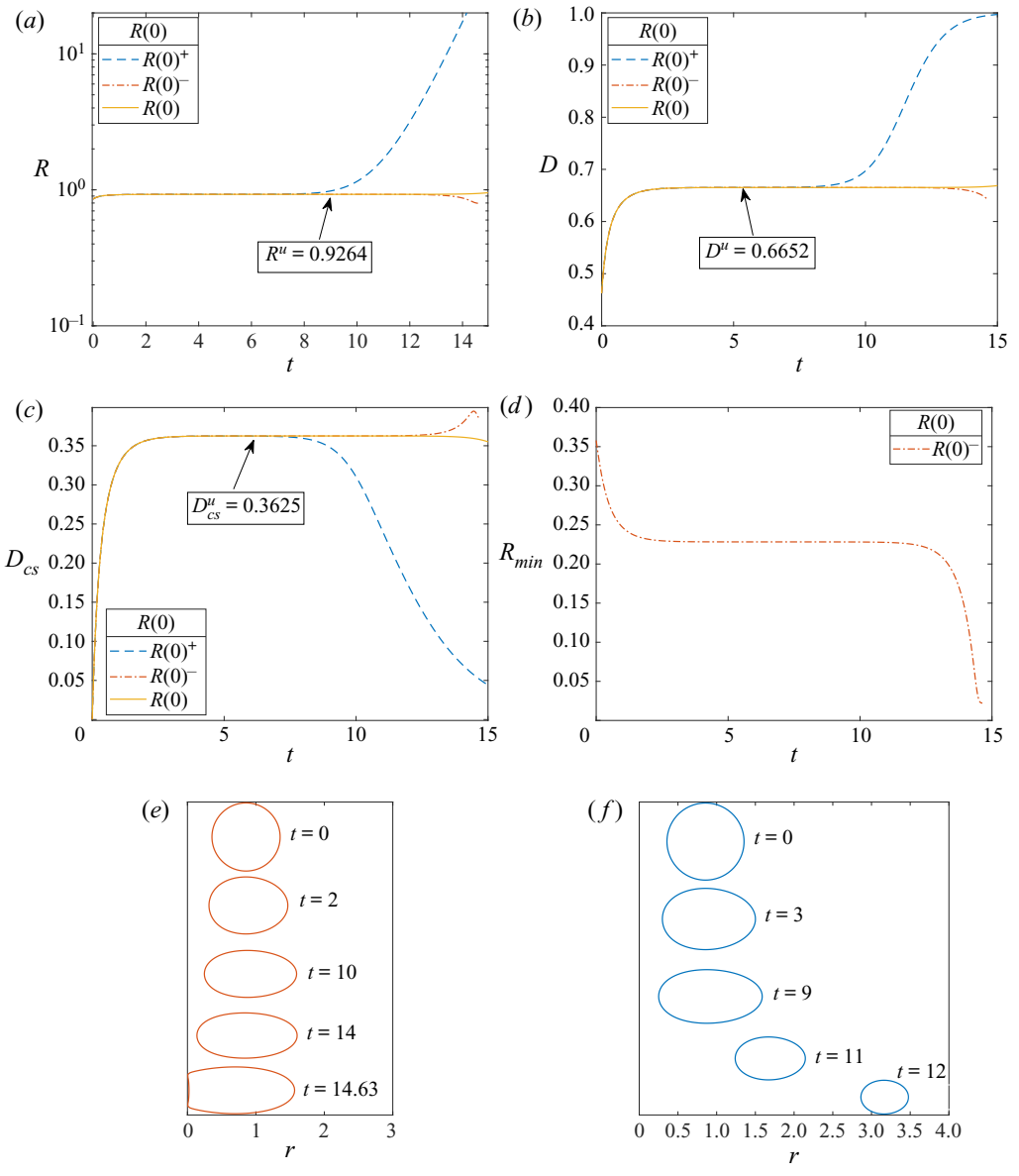

Figure 4. Dynamic evolution of parameters of a deforming torus, initially having circular cross-section, when $Bo = -1$ and $Ca = 0.21$. (*a*) Major radius of toroid. (*b*) Taylor deformation factor of the torus. (*c*) Deformation factor of the torus cross-section. (*d*) Minimum radius of torus. (*e*) Cross-section shapes of collapsing torus when $R(0) = R(0)^-$. (*f*) Cross-section shapes of expanding torus when $R(0) = R(0)^+$ where $R(0) = 0.855914357242$, $R(0)^+ = 0.8559144$ and $R(0)^- = 0.85591435723$.

stationary state and to prolong its existence before losing stability. Indeed, less accuracy in establishing this value, as is expected in experiments, will result in deviation from stationarity at shorter time. If the initial major radius exceeds the critical value R_c (see dashed lines in figures 4 and 5), the torus expands indefinitely. The cross-section first elongates along the r-axis while with the passage of time, as the toroid expands, D_{cs} diminishes toward the almost circular cross-section shape typical to a torus with large R.

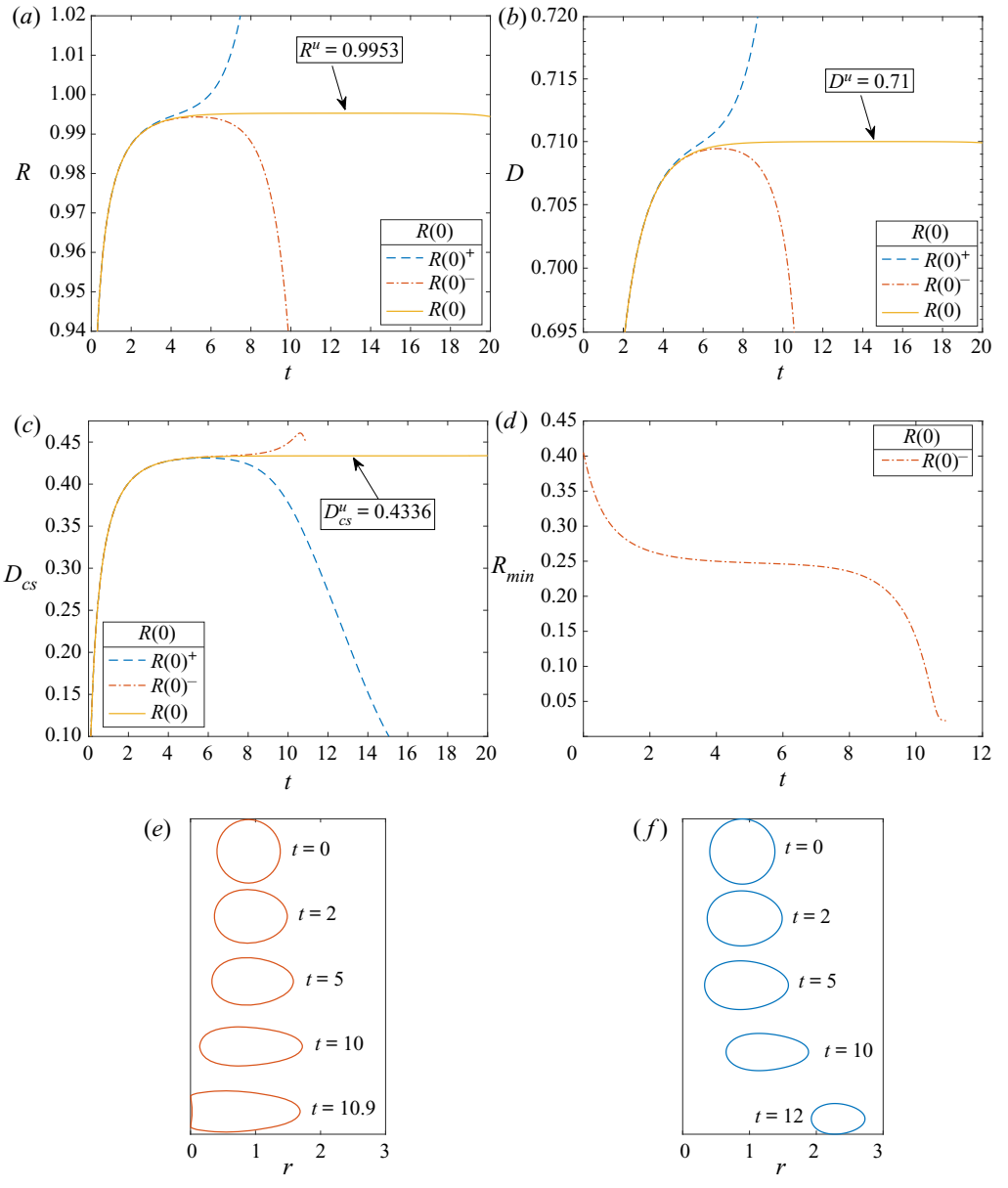

Figure 5. Dynamic evolution of parameters of a deforming torus, initially having circular cross-section, when $Bo = -3$ and $Ca = 0.3$. (*a*) Major radius of toroid. (*b*) Taylor deformation factor of the torus. (*c*) Deformation factor of the torus cross-section. (*d*) Minimum radius of torus. (*e*) Cross-section shapes of collapsing torus when $R(0) = R(0)^-$. (*f*) Cross-section shapes of expanding torus when $R(0) = R(0)^+$ where $R(0) = 0.8926018709$, $R(0)^+ = 0.89262$ and $R(0)^- = 0.892599$.

The value of R_c in this figure and in figures 5–7 relate to the curves marked by respective solid curve.

If the initial major radius $R(0)$ is less than R_c (see dashed–dotted lines in figures 4 and 5), following the initial expansion, the torus begins to shrink and eventually collapses towards the z-axis. Figure 4(*d*) represent the variation of R_{min} for the case of collapsing drop

with initial radius $R(0) = R(0)^-$. Here, R_{min} decreases with the initial increase in drop size, R, and the flattening of the cross-section. From $t = 4$ until $t = 10$, approximately, it shows negligible change, and after that period it tends to shrink as the torus collapses. Note the slight increase in R_{min} that can be observed near $t = 14.63$, which is due to the small pocket of outer fluid created near $r = 0$, that it is unable to be drained from the innermost part of the cross-section during the last stages of the collapsing dynamics, as it is shown in figure 4(*c*,*e*). Such capture is also evident in the video demonstration of axisymmetric collapse (Fragkopoulos *et al.* 2017) as can be seen in the last stages of cross-section approaching contact. Thus the first contact of total collapse is at some circle at $r = 0$ and $z \neq 0$. Similar behaviour of R_{min} is observed in figure 5(*d*). The evolution of the cross-section shapes corresponding to two regimes, collapsing and expanding is illustrated in figures 4(*e*,*f*) and 5(*e*,*f*). Finally, for $R(0) = R_c$, after initial increase in R and D and decrease in R_{min}, all of the parameters approach dynamic 'equilibrium' values and remain visibly constant for a relatively long time (solid curves). Note that after a certain time, following a slight disturbance as is, for example, an infinitesimal inaccuracy in $R(0)$, the drop either collapses or starts an indefinite expansion. This behaviour indicates the instability of the above mentioned equilibrium. These three dynamic regimes, collapse, expansion and stationarity, exist when the capillary number does not exceed some critical value, $Ca_c(Bo)$, while beyond the critical Ca, no equilibrium shapes are observed, and, hence, no stationary solutions were found. Note that, for a given Bo, as Ca approaches the critical value the time span of existing equilibrium becomes ever shorter until it completely diminishes at $Ca = Ca_c$. This behaviour is qualitatively similar to that reported in Zabarankin *et al.* (2015) and Ee *et al.* (2018) for the cases $Bo = 0$. Note also that in the case of heavy drops rotation and external compressional flow, combined, tend to expand the torus and resist the collapse caused by surface tension. As is shown below in § 6, all cases corresponding to compressional flow fail to yield a stationary stable shape.

5.2. *Rotating drops in extensional flow*

When the outer flow is extensional and tends to shrink the torus, no forcing exists that may lead to extension of a light toroidal drop and it collapses to the axis for any initial radius $R(0)$. The situation changes when a heavy rotating drop is exposed to an extensional flow. We performed simulations of such drops under extensional flow and examples of such results are presented below in figures 6 and 7.

Time evolutions of the parameters, R, D, D_{cs} and R_{min} for various initial major radius $R(0)$ with $Bo = 3$ and $Ca = -0.05$, and with $Bo = 1.0$ and $Ca = -0.025$ are shown in figures 6 and 7, respectively. Rather unexpected, in both figures, one can see the existence of two stationary shapes of the torus at radii, R^u and R^s where, $R^u < R^s$. Evidently (figures 6 and 7), in the case of extensional flow regime with heavy drops the toroidal drop may show dual stationary solutions corresponding to a single capillary number. The two cases in these figures differ in the distance between R^u and R^s which translates to different shapes of tori, their cross-sections and their dynamic evolutions. In figure 6(*a*) for $R_c = 3.4011$, the drop exhibits an unstable stationary solution when the drop's radius reaches the value $R^u = 3.401$ that is maintained from $t = 1$ to $t = 8$. Evolutions with $R(0)$ below R_c tend to collapse and with $R(0)$ above R_c show expansion. Nevertheless, this expansion does not proceed unbounded and it converges to a torus with $R^s = 5.82$ which continues to be stable for as long as the simulation proceeds. All dynamic evolutions initiating with $R(0) > R_c$, whether smaller or larger than $R = 5.82$, will converge to this R^s. Hence, starting the dynamics at R_c is required only for realizing the unstable solution,

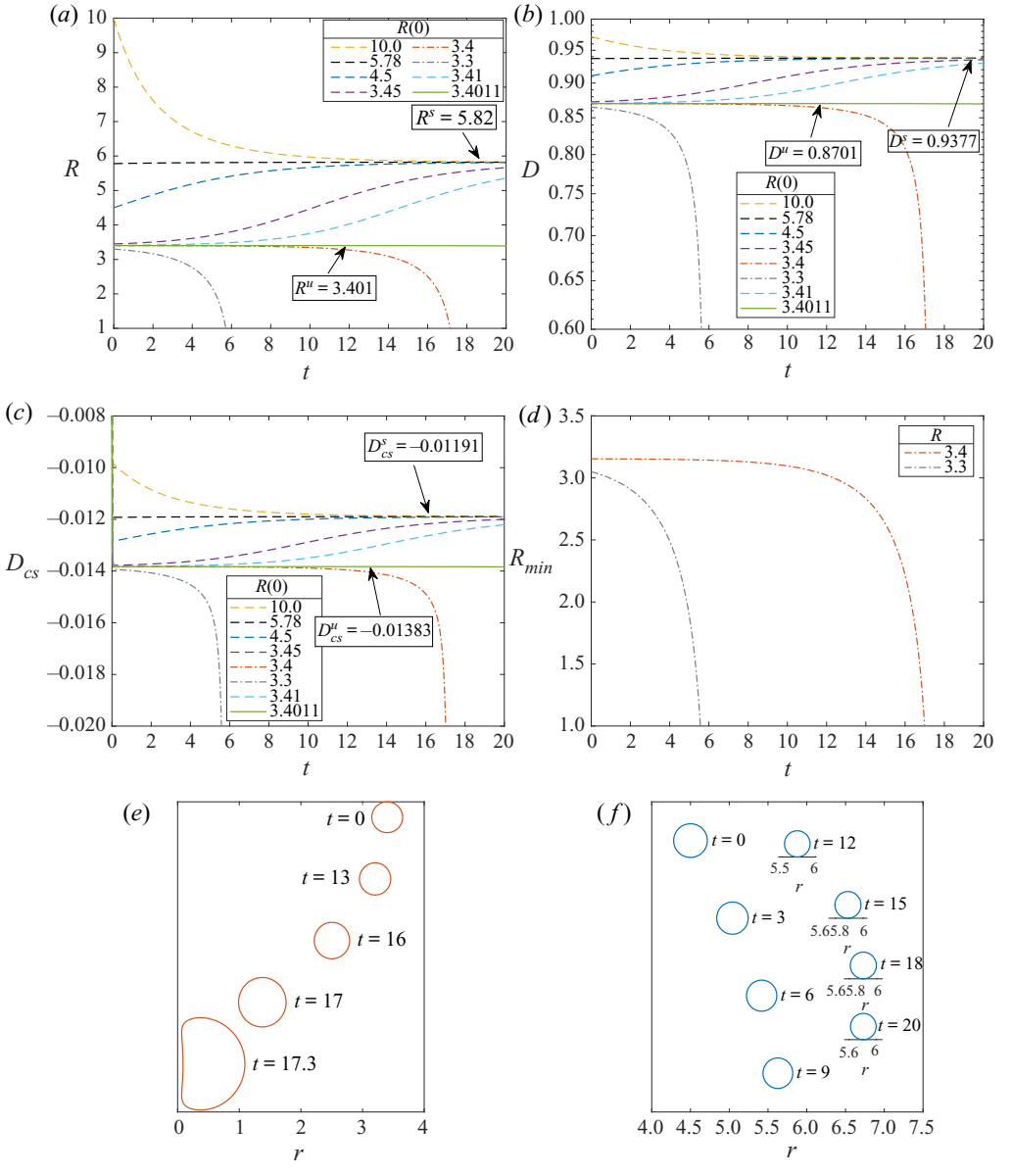

Figure 6. Dynamic evolution of parameters of a deforming torus, initially having circular cross-section, when $Bo = 1$ and $Ca = -0.025$. (*a*) Major radius of toroid. (*b*) Taylor deformation factor of the torus. (*c*) Deformation factor of the torus cross-section. (*d*) Minimum radius of torus. (*e*) Cross-sectional shapes of collapsing torus for $R(0) = 3.4$. (*f*) Cross-sectional shapes of expanding torus for $R(0) = 4.5$.

whereas, the stable solution is realized once obtained. This observation is also backed by figures 6(*b*) and 6(*c*) depicting the dynamic changes of D and D_{cs}. The dynamic collapse of cases starting at $R(0) < R_c$ and the corresponding shapes of the cross-section are depicted in figures 6(*d*) and 6(*e*). Here, we see that once the evolution departs from R^u the decrease of R_{min} is rather fast and the cross-section shape at almost total collapse is characterized by the enclosure of some external fluid near $z = 0$. Hence, as in the collapse during unsteady

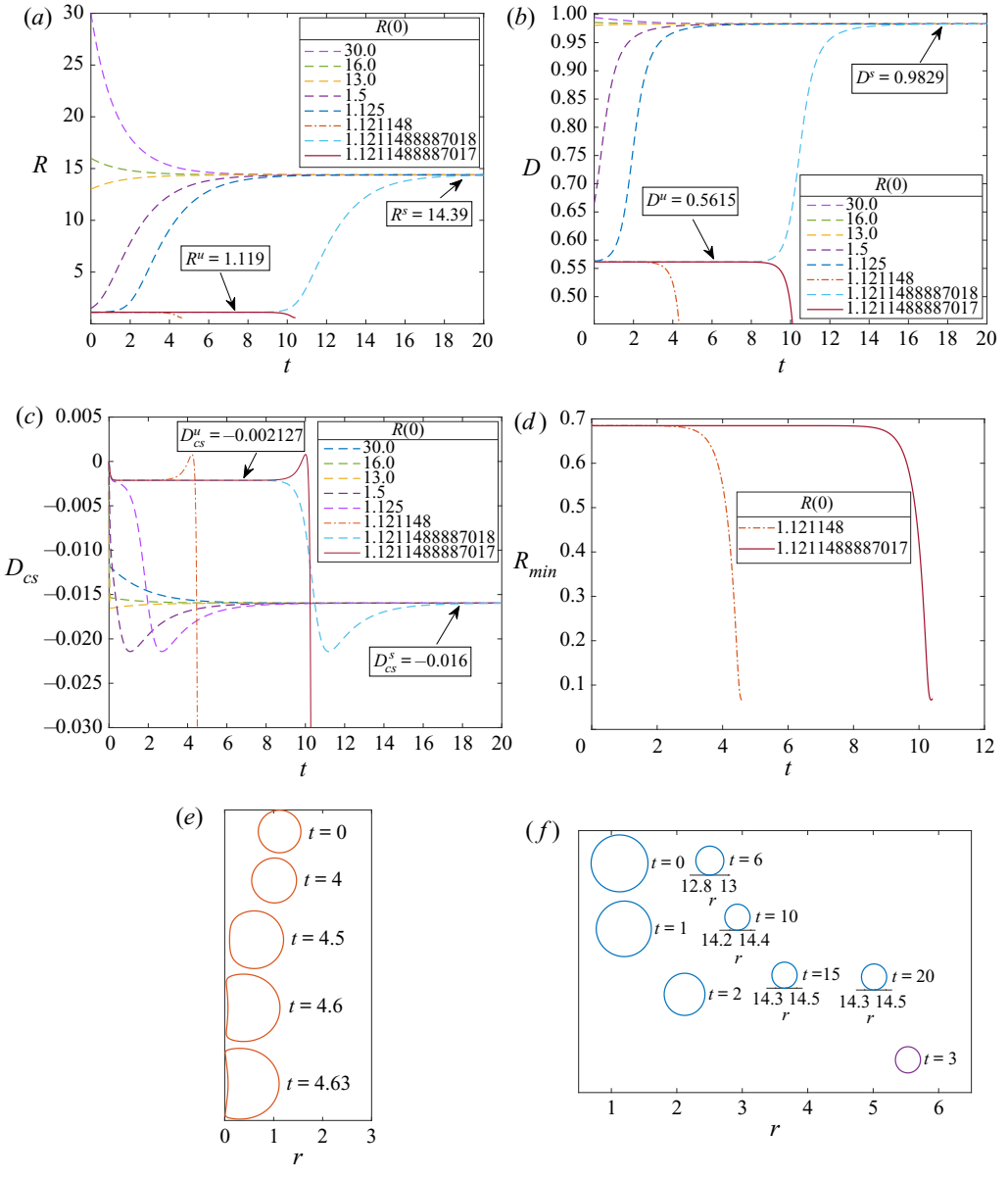

Figure 7. Dynamic evolution of parameters of a deforming torus, initially having circular cross-section, when $Bo = 3$ and $Ca = -0.05$. (*a*) Major radius of toroid. (*b*) Taylor deformation factor of the torus. (*c*) Deformation factor of the torus cross-section. (*d*) Minimum radius of torus. (*e*) Cross-sectional shapes of collapsing torus for $R(0) = 1.121148$. (*f*) Cross-sectional shapes of expanding torus for $R(0) = 1.125$.

dynamics in the case of compressional flow, the first contact in the inner region of the torus is at a circle at $z \neq 0$ and $r = 0$. The cross-section shapes of the torus undergoing expansion from the unsteady shape to the steady one are depicted in figure 6(*f*) where it is clear that they gradually converge to an oval that is almost circular.

Similar dynamic evolution is shown in figure 7. Two stationary solutions are obtained, one unstable at $R^u = 1.119$ and one stable solution at $R^s = 14.39$. Here too, the dynamics

of expanding tori from the unsteady shape eventually converges to the stable steady torus with almost circular cross-section, as is depicted in figures 7(*a*), 7(*b*) and 7(*f*), while the collapsing tori show a similar fast approach of R_{min} to the z-axis and a similar evolution of the cross-section shape, particularly at contact. There is, however, a difference in the cases shown in figures 6 and 7. It is a result of the distance between R^u and R^s in each respective case. Note that in figure 6 the stable and unstable tori are relatively close to each other, while in figure 7 we presented a case in which the radius R^s of the steady torus is an order of magnitude larger than that of the unsteady one. Indeed, in as much as the dynamic expansion from the unsteady torus to the steady one, we see no major dynamic differences. The evolution, governed by the viscous forces, approaches the steady solution monotonically as is shown in figures 6(*c*) and 6(*f*). Similarly, the stages of collapse, that follow an evolution starting at $R(0) = 3.4$ (slightly less than 3.4011), resemble those encountered in collapse associated with compressional flow.

However, there is a considerable difference in the deformation factors of the cross-sections and their dynamics, in figures 6 and 7. In figure 6(*c*), $D^u_{cs} < D^s_{cs}$, while in figure 7(*c*), $D^u_{cs} > D^s_{cs}$. The dynamics of transfer from the unsteady solution to the steady one, in the case of figure 6, does not involve major changes in the cross-section shape and, thus, surface tension plays a minor role and the transition is monotonic and smooth as is shown in figure 6(*c*). However, in the case depicted in figure 7, the cross-section shape in the unsteady torus is an almost perfect relatively large circle. The transition to the steady state involves a considerable shrinking of the almost circular cross-section with the acting surface forces affected by an ever increasing local curvature. Indeed, the evolution in expansion (or collapse) depicted in figure 7(*c*) shows nonlinear dynamic effects rendered by capillarity, with local minima and maxima appearing along the processes. Figures 7(*e*) and 7(*f*) show the shape of cross-sections of the collapsing and stable stationary drops, respectively. The dynamic cross-section deformation, corresponding to the initial radius $R(0) = 1.121148$, is shown in figure 7(*e*) where the major radius shrinks while the cross-sectional area increases. Finally, the torus collapses towards the centre after $t \simeq 4.0$. The cross-sectional shapes of stationary stable drop are shown for the case when $R(0) = 1.125$ in figure 7(*f*), and the drop radius extends until it attains a stable stationary state. In § 6 we present maps showing the subregions in which steady and unsteady stationary solutions exist and their relation with relevant singly connected branches reported by Malik *et al.* (2020).

6. Stable and unstable stationary axisymmetrically rotating drops under the influence of compressional or extensional flow

This section is devoted to a summary report of stationary shapes of the toroidal drop in a linear flow that combines axisymmetric shear and rotation, in terms of the physical parameters, Taylor deformation factor and capillary and Bond numbers. Recall that, in this paper, positive Ca corresponds to compressional flow while negative Ca is used to describe extensional flow. Positive and negative Bo indicate a drop with the density higher or lower than that of the ambient fluid, respectively.

6.1. *Rotating drop in compressional flow*

In figure 8 the Taylor deformation factor D defined in (3.7) is plotted versus the capillary number for a variety of Bond numbers. Evidently, for each value of the Bond number there exist a critical capillary number, $Ca_c(Bo)$, beyond which no stationary solutions are found. This critical capillary number decays with the growth of Bo. For a light drop and

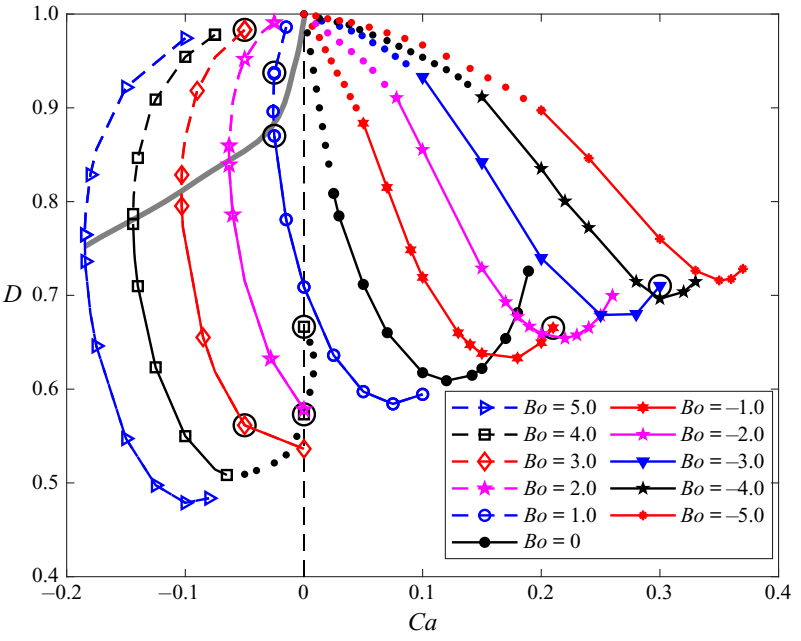

Figure 8. Phase plane of stable and unstable stationary toroidal drops rotating in axisymmetric linear flow. Here $Ca > 0$ and $Ca < 0$ denote compressional and extensional flow, while $Bo > 0$ and $Bo < 0$, refer to heavy and light drops, respectively. Circled points are special cases discussed in § 5.

subcritical intensity of compressional flow ($0 < Ca < Ca_c(Bo), Bo \leq 0$) only one toroidal stationary shape exists, that was shown to be unstable in our simulations. In the case of a light drop, both the centrifugal force and the surface tension tend to shrink the toroid. Thus, the more intensive is the rotation (higher $|Bo|$), the more intensive compressional flow (higher Ca) is required to resist this collapse, thereby increasing the tendency of the unstable tori to expand indefinitely. Thus, light drops require stronger compressional flow to maintain stationarity and such cases are more susceptible to loose stability. In contrast to this, when the drop is heavier than the ambient fluid, $Bo > 0$, the centrifugal force tends to expand the torus. The critical Ca diminishes with the growth of rotation intensity, and for high enough Bond number, no equilibrium shapes are found under compressional flow. These are the cases depicted in figure 8 in the subregion $Ca > 0$.

6.2. *Heavy drops in extensional flow*

When the outer flow is extensional, it tends to shrink the torus. Under such a flow no forcing exists that may lead to an expansion of a light toroidal drop and it therefore collapses to the axis for any initial radius. For a heavy drop under extensional flow, the interplay of surface tension, centrifugal force and shear results in two possible stationary states for a pair (Ca, Bo). Our simulations demonstrate that shapes with lower major radius are unstable, while those with higher radius, do not change for an indefinitely long time. This suggests that it is stable with respect to axisymmetric disturbances. We address these shapes as stable, though we did not perform analytical stability analyses. In figure 8 unstable solutions are denoted by solid curves and stable shape are shown by dashed curves.

For each intensity of the rotation ($Bo > 0$) there is a negative critical Ca_{cr}, under which the shrinking effect of surface tension and extensional outer flow dominates over the expanding effect of rotation for any torus shape. Thus at a given Bo, for $Ca < Ca_{cr}$ no stationary shapes are found. This is similar to the other extreme in the case of compressional flow when $Ca > Ca_c$. Here, for any constant value of the rotation intensity, Bo, there is an interval of capillary number defined by

$$Ca_{cr}(Bo) < Ca < Ca_c(Bo), \tag{6.1}$$

in which stationary solutions are found. The solutions within these boundaries may contain all possible combinations of relative drop density and compressional or extensional flow. In figure 8 stable and unstable solutions connecting values of $Ca_{cr}(Bo)$ are divided by a thick line. Stable solutions are in the upper left region above this line. This indicates that stable solutions are possible only for heavy drops under extensional flow. In this subregion, the rotation aims to expand the torus while extension and surface tension act to restrain this expansion, and the equilibrium is stable as is evident in the dynamic calculations. In the rest of the parameters' domain the combined action of rotation and shear results in an equilibrium that is unstable. It is sensitive to any infinitesimal perturbation that grows to send the torus to collapse or expand either to infinity or to merge onto a stable equilibrium. Note that the two starred points of figure 2, at $Bo = 4$ and 4.0004, are transferred to figure 8 at $Bo = 0$ and at $Ca = 0$ due to the change in the value of the normalizing velocity, which is proportional to G in this section.

6.3. *Description of fluid flow*

In this subsection we describe the fluid flow under the combined effect of rotation and compressional or extensional linear flow. We start with the undisturbed flow. In the laboratory frame and with the absence of rotation, the stream surfaces are hyperbolic concentric envelopes surrounding the axis of rotation. Progressing along such an envelope, from large z to smaller z, it widens in the r direction. At large r these surfaces are almost parallel to each other asymptotically approaching the $z = 0$ plane. Particle paths on these surfaces will look like a bundle of spaghetti noodles. Adding a rotation about the axis of symmetry, the structure of the envelopes as concentric surfaces will not be altered, however, the path lines (streak lines) on them will be twisted along the rotational velocity component as their radial distance increases. Next, when inserting a torus centred at the origin and symmetric about the $z = 0$ plane, the structure of the envelopes in the outer flow is expected to be distorted, reflecting the surface shape.

We next address the torus surface and internal streak lines in the laboratory frame. In the absence of rotation, when vertical cross-section is observed, they will look like close loops, (see, e.g. Zabarankin *et al.* 2015). In compressional flow the streak line progresses from R_{min} to R_{max} on the surface and retracts within the torus on the $z = 0$ plane to meet the same point at the torus inner R_{min} circle. Inner streak lines are enclosed within the surface one. However, when rotation exists the particle on the surface streak line is continuously pushed in the rotational direction, and when it approaches back toward the torus inner circle it will be at a different point depending on the intensity of the shear (Ca) and the rotation (Bo). The inner paths of particles will experience the same effect of rotation. A schematic plot of the spiral structure of a surface streak line is depicted in figure 9, where a segment of the circular torus is schematically spread. In this figure the progress of the particle on the path line follows a compressional flow component. For extensional flow component, the arrows on the steak line should be inverted, but the structure

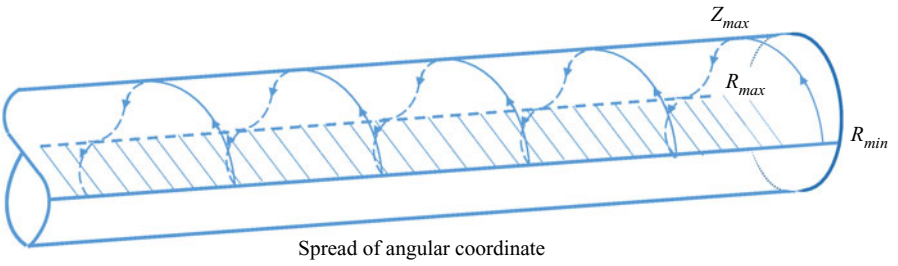

Figure 9. Schematic plot of a streak line on a stationary surface for compressional flow combined with rotation.

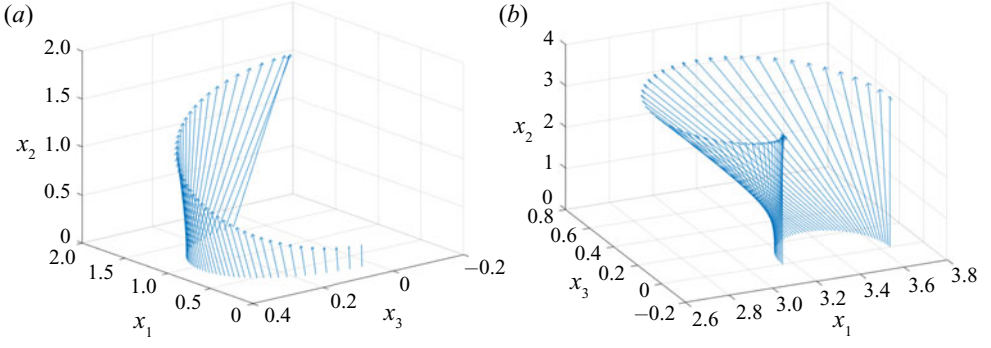

Figure 10. The intensity of the surface tangential velocity between R_{min} and R_{max} shown in laboratory frame. (*a*) Rotation and compression at $Ca = 0.21$, $Bo = -1$ and $R = 0.85591$. (*b*) Rotation and extension at $Ca = -0.025$, $Bo = 1$ and $R = 3.4011$.

remains similar. These apply of course only to stationary states where the flow and the surface structure remain unchanged in time.

In figure 10 we present examples showing the tangential velocity vectors along a cross-section of the exposed surface in the laboratory frame, spanning the surface interval between R_{min} at the inner circle and R_{max} at the outer one. The two examples, figures 10(*a*) and 10(*b*), demonstrate the tangential velocity of rotation, combined with compressional or extensional shear, respectively. Those are demonstrated in the unstable stationary cases depicted in figures 4 and 6. The length of the arrows simulates the intensity of the vector in which, for the purpose of demonstration only, the rotational component is rescaled by ω, i.e. $\omega/G = 1$. The presented tangential velocity components apply just as well along a streak line in the axisymmetric stationary state since all values of tangential velocity, at a constant radial position on the surface, are the same. Note also the vectors approaching the pole R_{max}, that seem inclined backward. These are not in error as they tend to become oriented parallel to the vertical coordinate where the tangential velocity is in the direction of rotation.

The schematic description in figure 9 suggest a continuous non-zero value for the surface tangential velocity vector. This is indeed verified in the examples depicted in figure 10. This description indicates that there is no point of separation of streak line at the surface or of the external streamlines. Indeed, for the non-rotating cases, when $Bo = 0$, Ee *et al.* (2018) demonstrated that there will be no such separation at all Ca, for the torus viscosity equal to, and less or greater than, the viscosity of the outer fluid. Below, in figure 11, we present several such calculated values of the tangential velocity in rotational coordinates

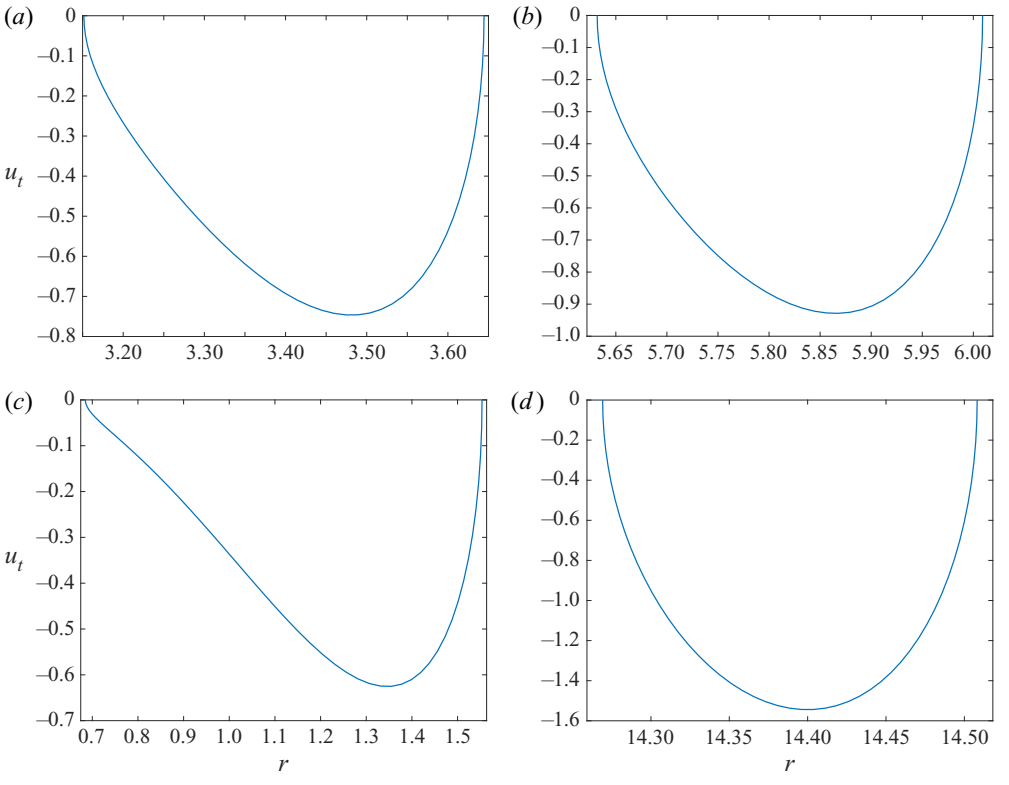

Figure 11. Tangential velocity (u_t) in rotating coordinate frame on surface of stationary shapes in rotation and extension. (a,b) Unsteady and steady cases at $Bo = 1$ and $Ca = -0.025$, $R = 3.4011$ and 5.78, respectively. (c,d) Unsteady and steady cases at $Bo = 3$ and $Ca = -0.05$, $R = 1.12115$ and 16.0, respectively.

frame, at Bo not equal to zero, demonstrating that a similar phenomenon of no separation exits also in the presence of the additional rotation. These examples in figure 11 are shown in cases involving rotation and extension, when dual solutions exist for the same Bo and Ca values. It is seen that there is no difference in the structure of surface tangential velocity indicating similar flow structure for both unsteady and steady stationary cases. The values in the case figure 11(d) are somewhat higher than those in figure 11(c) since the torus is more expanded in the radial direction. The appearance of axisymmetric stability at these expanded tori, affected by the balance of rotation and expansion, may reflect a strong capillary force acting on a small almost circular cross-section, with a much higher curvature compared with the diminishing curvature of torus radius.

6.4. *Special points*

Some points in figure 8 deserve special attention. They are marked in extra circles. Note the two points on the right-hand side of the figure. They belong to the curves of unstable stationary solutions of the cases $Bo = -1$ and $Bo = -3$ depicted and discussed in § 5 in figures 4 and 5. They are the most extreme calculations we could safely perform for tori, all in compressional flow before collapse, though somewhat short of Ca_c for these cases.

For the cases of rotating heavy drops subjected to extensional flow we marked two points on the $Bo = 1$ curve and two on the $Bo = 3$ curve. The former two points are at $Ca = -0.025$ and the dual solution are relatively close on both sides of the dividing line of Ca_{cr},

separating the steady and unsteady solutions for $Bo = 1$. These solutions are discussed in § 5, in figure 6. The latter two points at $Bo = 3$, are relatively far apart and are the cases discussed there in figure 7.

Note that for the case of $Bo = 4$ the last point of unsteady solution evaluated by the BIE method is at $Ca = -0.07$. Nevertheless, we can associate with this case two more points from figure 2 (with $Ca = 0$) at $Bo = 4$ (lower point) and at $Bo = 4.0004$ (upper point at total collapse). With these two additions we can estimate the curve of the case $Bo = 4$ and this interpolation is illustrated by the black points.

The last special point that is worth mentioning is the one designated by $Ca = 0$ and $D = 1$. This is the limit to which all unsteady tori in compressional flow are aiming at and it is also the Ca_{cr} for all the compression cases in the inequality (6.1). This point is also the limiting point of all steady tori in extensional flow. At this point the limiting torus radius is $R \to \infty$ and it has a circular cross-section of zero area. It is the 'black hole' of all rotating tori embedded in axisymmetric linear flows.

6.5. *Multiplicity of solution*

The branches denoting stationary solutions showing toroidal shapes are associated with branches showing stable singly connected drops obtained by Zabarankin *et al.* (2013), Ee *et al.* (2018) and Malik *et al.* (2020). The former two investigated compressional flow without rotation, $Bo = 0$, for various values of the viscosity ratio, while Malik *et al.* (2020) extended their domain to span the entire region of stable stationary solutions, including also extensional flow components for negative and positive values of Bo. The stable rotating singly connected drops are shown in the interval $Ca_l \leq Ca \leq Ca_r$ in the nomenclature definition of Malik *et al.* (2020). Our definition will yield $-Ca_r \leq Ca \leq -Ca_l$ using their values. Examples of such calculated two types of branches, singly connected and toroidal, are depicted in figure 12 for the cases $Bo = -3,\ 0$ and 4. Note that in these cases we incorporated points, taken from figure 2 and from Malik *et al.* (2020), marked by circled asterisks. The branches arrive at close proximity but do not show a joint point, mainly because of the numerical difficulties encountered in obtaining unsteady heavily dimpled flat drops as well as almost completely collapsed tori (with $R_{min} \to 0$). These gaps that may contain segments that connect the two branches deserve separate attention as they can be completed by combining a special approximated method with BIE calculations (Lavrenteva *et al.* 2021). Examples of deformation curves containing both simply connected and toroidal branches are presented in figure 12. We observe that there is a gap between the last calculated point of the flat drop (calculated at $|Ca_l|$, beyond which no stable dimpled drop exists) and the last point of the almost collapsed stationary unstable toroidal drop (for which stationarity could still be assumed). This gap is augmented with the increase of $|Bo|$ and is, thus, common to heavy and light drops as well.

The case $Bo = 4$ contain two points taken from figure 2 on the vertical line $Ca = 0$ that deserves special attention and is detailed in figure 13. It is evident that the curve of $Bo = 4$ must cross the $Ca = 0$ vertical line into the compressional zone at the lower point, and turn back toward the extensional zone at the upper point, thereby suggesting a turning location for Ca_c for this case at approximately $Ca_c \approx 0.005$ and deformation factor of $D \approx 0.63$. Estimated interpolations are marked by solid dots. The upper dot on the $Ca = 0$ line is also a point denoting the collapse into a singly connected shape. Hence, the point of maximum existence of singly connected drop at Ca_l and the point of its collapse to toroidal shape at $Ca = 0$ were also connected by an estimated interpolation marked by solid dots. More exact approximation of these interpolated dots, connecting these segments of highly unstable stationary solutions, require a hybrid approach employing BIE and a

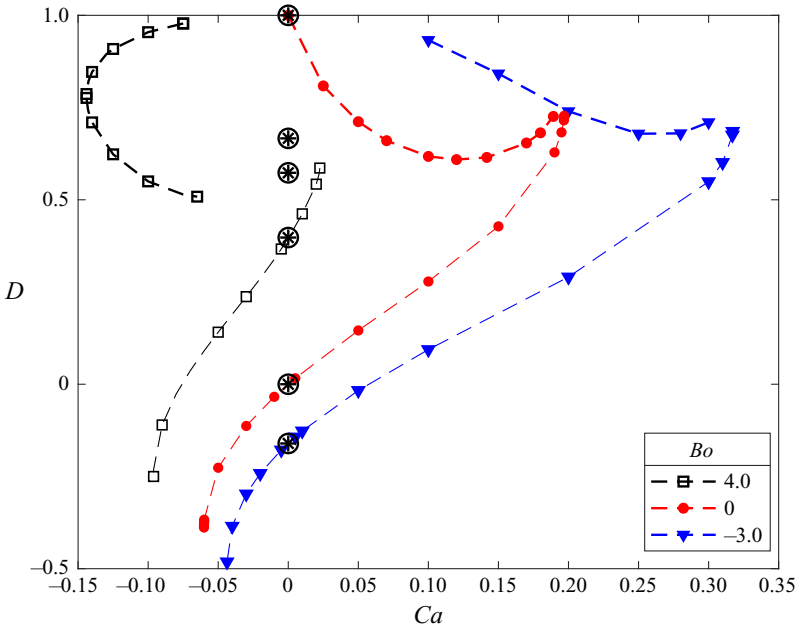

Figure 12. Examples of branches of stationary toroidal and associated stable singly connected drops when the cases $Bo = 4,\ 0$ and -3. Circled points are obtained from figure 2.

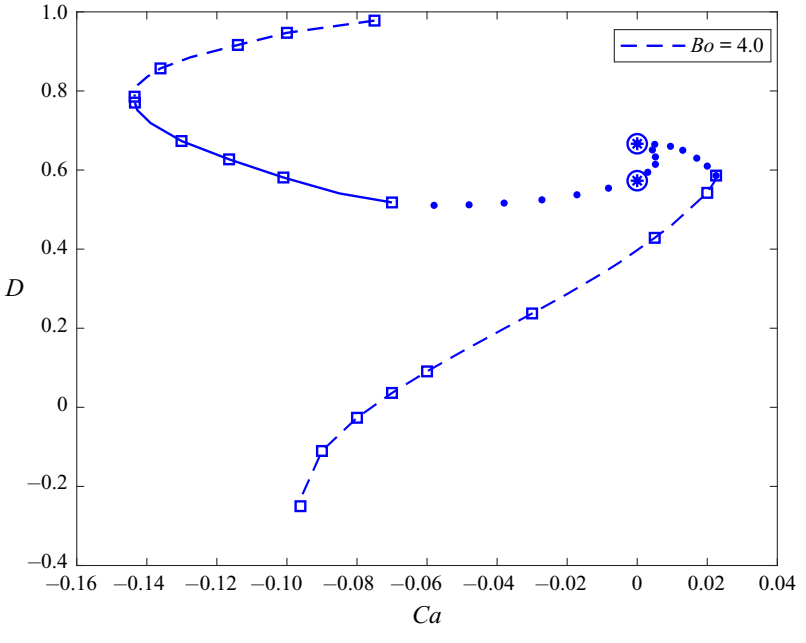

Figure 13. Map of stationary solutions for the special case $Bo = 4$. The dashed line denotes calculated stable toroidal and singly connected drops; the solid line denotes calculated unsteady toroidal drops; solid dots are approximate interpolation; circled points are obtained from figure 2.

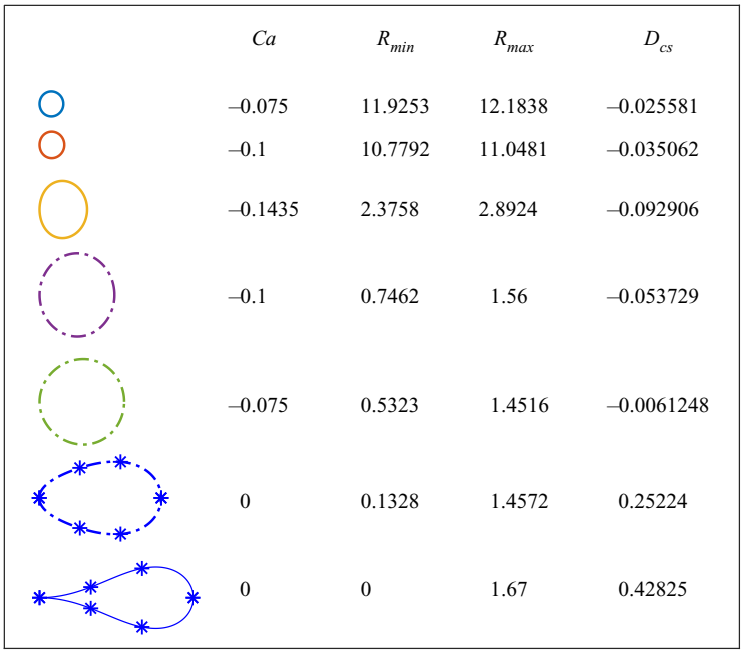

Figure 14. Cross-sections of stationary shapes of toroidal drops for $Bo = 4$ at various Ca. The top three are stable and the bottom four are unstable.

special estimate of shapes, as was recently suggested for the case $Bo = 0$ (Lavrenteva *et al.* 2021).

It is interesting to note the expected multiplicity of solutions for this case, $Bo = 4$. In addition to the stable stationary singly connected drop, we find in the interval $-0.1435 = Ca_{cr} < Ca < 0$ two toroidal shapes, a stable torus and an unstable one, both in extensional flow. Farther in the interval $0 < Ca < Ca_c \approx 0.005$ we find two toroidal shapes both unstable in compressional flow. Beyond Ca_c in the interval $Ca_c < Ca < -|Ca_l| = 0.02252$ we expect only two singly connected drops, a stable one and an unstable dimpled one.

The various stationary shapes associated with the case $Bo = 4$ are depicted in figure 14. It is interesting to observe that the cross-sections of the toroidal shapes are mostly oval. In the stable tori subregion these ovals are very close to circular where the vertical dimension only slightly exceeds the horizontal one, $z_{max} > (R_{max} - R_{min})/2$ or $D_{cs} < 0$. Near the transition from stable to unstable shapes the cross-section vertical orientation of the ellipse becomes more pronounced with the least D_{cs} observed. However, when one proceeds to examine more collapsed torus shapes as the shear flow turns from extensional to compressional, the cross-section major oval direction changes to horizontal and, near the collapse region of the stationary torus it acquires an egg shape with the higher curvature near R_{min} with $D_{cs} = 0.42825$.

7. Discussion and conclusion

In this paper we presented a numerical study of dynamic and of stationary deformation patterns of toroidal drops embedded in a viscous flow field, combined of rotation and axisymmetric linear shear, compressional or extensional.

It is demonstrated that under a compressional (biextensional) flow the behaviour of a rotating toroidal drop is qualitatively similar to that in the absence of rotation (studied in Zabarankin *et al.* 2015; Ee *et al.* 2018). Namely, when the viscous forces that are proportional to the intensity of the shear, are relatively weak compared with the surface tension (the ratio of these forces is characterized by the capillary number, Ca), three different scenarios of drop evolution are possible: indefinite expansion of the liquid torus, contraction to the centre and a stationary toroidal shape. For capillary numbers greater than a critical value, depending on the intensity of rotation $Ca_c = Ca_c(Bo)$, no stationary toroidal shapes are found.

In the case of a light drop (with density less than that of the ambient fluid, $Bo < 0$), the centrifugal force tends to shrink the toroid, i.e. it acts together with surface tension against the compressional flow. Thus, the more intensive the rotation is (higher $|Bo|$), the more intensive compressional flow (higher Ca) is required to overcome this tendency and make the torus expand dynamically to indefinitely. The critical capillary number increases with the absolute value of Bo. In contrast to this, when the drop is heavier than the ambient fluid, $Bo > 0$, the centrifugal force tends to expand the torus. The critical Ca diminishes with the growth of rotation intensity, and for high enough Bond number, no equilibrium shapes are found under compressional flow.

The situation changes when the outer flow is extensional and tends to shrink the torus. Under such a flow no forcing exists that may lead to an expansion of a light toroidal drop, and it collapses to the axis for any initial radius. For a heavy drop a multiplicity of stationary toroidal shapes exists. These branches are an addition to branches of singly connected drop shapes reported by Malik *et al.* (2020). When rotation is combined with extensional flow, a considerable subdomain of Bond and capillary numbers with stable stationary solutions, implying stable tori, does exist. The existence of stable toroidal deformation was a primary objective of this effort. For each positive value of Bo (heavy drops in extensional flow) there exists a critical negative capillary number, Ca_{cr}, under which no stationary solutions were found. The line collecting these critical values $Ca_{cr}(Bo)$ denotes the boundary between the zones of stable and unstable toroidal shapes. The lower subdomain of a combination of rotation and extensional flow, and the entire domain in which rotation and compressional flow are combined, result in stationary solutions, all of them yielding unsteady shapes. It is noted that the latter branches are approaching branches of singly connected flat drops having the same Bo. The connection of these branches is yet to be resolved and calculated.

It is interesting to compare the dynamics with that observed when different forcing is present. Fragkopoulos & Fernández-Nieves (2017) presented an experimental study of the dynamics of charged toroidal drop. The charging tends to expand the torus and to prevent its collapse to the centre. However, in their experiments, when collapse is hindered, tori always end up breaking into spherical droplets due to Rayleigh–Plateau instability.

Recall that we term the solution unstable if with passage of time it is destroyed by the development of unavoidable numerical disturbances, and stable if it can persist indefinitely. This suggest instability or stability with respect to axisymmetric disturbances, while the effect of non-axisymmetric ones that may result in the development of the Rayleigh–Plateau instability is yet to be studied.

Funding. This work is supported by the Israel Science Foundation (grant no. ISF 1207/18). O.M.L. also acknowledges the support of a joint grant from the Center for Absorption in Science of the Ministry of Immigrant Absorption and the Committee for Planning and Budgeting of the Council for Higher Education under the framework of the KAMEA Program.

Declaration of interests. The authors report no conflict of interest.

Author ORCIDs.
Sumit Malik https://orcid.org/0000-0001-5178-7884;
O.M. Lavrenteva https://orcid.org/0000-0001-9115-0677;
A. Nir https://orcid.org/0000-0002-8166-2406.

References

AN, D., WARNING, A., YANCEY, K.G., CHANG, C.-T., KERN, V.R., DATTA, A.K., STEEN, P.H., LUO, D. & MA, M. 2016 Mass production of shaped particles through vortex ring freezing. *Nat. Commun.* **7** (1), 1–10.

AUSSILLOUS, P. & QUÉRÉ, D. 2004 Shapes of rolling liquid drops. *J. Fluid Mech.* **512**, 133.

BAUMANN, N., JOSEPH, D.D., MOHR, P. & RENARDY, Y. 1992 Vortex rings of one fluid in another in free fall. *Phys. Fluids* A **4** (3), 567–580.

CHAMPION, J.A., KATARE, Y.K. & MITRAGOTRI, S. 2007 Particle shape: a new design parameter for micro-and nanoscale drug delivery carriers. *J. Control Release* **121** (1–2), 3–9.

CHANG, Y.-W., FRAGKOPOULOS, A.A., MARQUEZ, S.M., KIM, H.D., ANGELINI, T.E. & FERNÁNDEZ-NIEVES, A. 2015 Biofilm formation in geometries with different surface curvature and oxygen availability. *New J. Phys.* **17** (3), 033017.

CHEN, C.-H., SHAH, R.K., ABATE, A.R. & WEITZ, D.A. 2009 Janus particles templated from double emulsion droplets generated using microfluidics. *Langmuir* **25** (8), 4320–4323.

DEAN, D.M., NAPOLITANO, A.P., YOUSSEF, J. & MORGAN, J.R. 2007 Rods, tori, and honeycombs: the directed self-assembly of microtissues with prescribed microscale geometries. *FASEB J.* **21** (14), 4005–4012.

DESHMUKH, S.D. & THAOKAR, R.M. 2013 Deformation and breakup of a leaky dielectric drop in a quadrupole electric field. *J. Fluid Mech.* **731**, 713–733.

EE, B.K., LAVRENTEVA, O.M., SMAGIN, I. & NIR, A. 2018 Evolution and stationarity of liquid toroidal drop in compressional stokes flow. *J. Fluid Mech.* **835**, 1–23.

FONTELOS, M.A., GARCIA-GARRIDO, V.J. & KINDELÁN, U. 2011 Evolution and breakup of viscous rotating drops. *SIAM J. Appl. Maths* **71** (6), 1941–1964.

FRAGKOPOULOS, A.A. & FERNÁNDEZ-NIEVES, A. 2017 Toroidal-droplet instabilities in the presence of charge. *Phys. Rev.* E **95** (3), 033122.

FRAGKOPOULOS, A.A., PAIRAM, E., BERGER, E., SEGRE, P.N. & FERNÁNDEZ-NIEVES, A. 2017 Shrinking instability of toroidal droplets. *Proc. Natl Acad. Sci. USA* **114** (11), 2871–2875.

GHAZIAN, O., ADAMIAK, K. & CASTLE, G.S.P. 2013 Numerical simulation of electrically deformed droplets less conductive than ambient fluid. *Colloids Surf.* A **423**, 27–34.

HEINE, C.-J. 2006 Computations of form and stability of rotating drops with finite elements. *IMA J. Numer. Anal.* **26** (4), 723–751.

HYND, R. & MACCUAN, J. 2006 *On Toroidal Rotating Drops*. Niedersächsische Staats-und Universitätsbibliothek.

KOJIMA, M., HINCH, E.J. & ACRIVOS, A. 1984 The formation and expansion of a toroidal drop moving in a viscous fluid. *Phys. Fluids* **27** (1), 19–32.

LAVRENTEVA, O.M., EE, B.K., SMAGIN, I. & NIR, A. 2021 Approximating stationary deformation of flat and toroidal drops in compressional viscous flow using generalized Cassini ovals. *J. Fluid Mech.* **921**, A5.

MACHU, G., MEILE, W., NITSCHE, L. & SCHAFLINGER, U. 2001*a* The motion of a swarm of particles travelling through a quiescent, viscous fluid. *Z. Angew. Math. Mech.* **81** (S3), 547–548.

MACHU, G., MEILE, W., NITSCHE, L.C. & SCHAFLINGER, U.W.E. 2001*b* Coalescence, torus formation and breakup of sedimenting drops: experiments and computer simulations. *J. Fluid Mech.* **447**, 299.

MALIK, S., LAVRENTEVA, O.M. & NIR, A. 2020 Shapes and stability of viscous rotating drops in a compressional/extensional flow. *Phys. Rev. Fluids* **5** (2), 023604.

MEHRABIAN, H. & FENG, J.J. 2013 Capillary breakup of a liquid torus. *J. Fluid Mech.* **717**, 281.

MENCHACA R, A., BORUNDA, M., HIDALGO, S.S., HUIDOBRO, F., MICHAELIAN, K., PÉREZ, A. & RODRÍGUEZ, V. 1996 Are the toroidal shapes of heavy-ion reactions seen in macroscopic drop collisions? *Revista Mexicana de Fisica* **42** (suppl. 1), 198–202.

NURSE, A., FREUND, L.B. & YOUSSEF, J. 2012 A model of force generation in a three-dimensional toroidal cluster of cells. *J. Appl. Mech.* **79** (5), 051013.

NURSE, A.K., CORIELL, S.R. & MCFADDEN, G.B. 2015 On the stability of rotating drops. *J. Res. Natl Inst. Stand. Technol.* **120**, 74–101.

PAIRAM, E. & FERNÁNDEZ-NIEVES, A. 2009 Generation and stability of toroidal droplets in a viscous liquid. *Phys. Rev. Lett.* **102** (23), 234501.

PAIRAM, E., VALLAMKONDU, J., KONING, V., VAN ZUIDEN, B.C., ELLIS, P.W., BATES, M.A., VITELLI, V. & FERNANDEZ-NIEVES, A. 2013 Stable nematic droplets with handles. *Proc. Natl Acad. Sci. USA* **110** (23), 9295–9300.

PLATEAU, J. 1857 I. Experimental and theoretical researches on the figures of equilibrium of a liquid mass withdrawn from the action of gravity–third series. *Lond. Edinb. Dublin Phil. Mag. J. Sci.* **14** (90), 1–22.

POZRIKIDIS, C. 1992 *Boundary Integral and Singularity Methods for Linearized Viscous Flow*. Cambridge University Press.

RALLISON, J.M. & ACRIVOS, A. 1978 A numerical study of the deformation and burst of a viscous drop in an extensional flow. *J. Fluid Mech.* **89** (1), 191–200.

RENARDY, Y., POPINET, S., DUCHEMIN, L., RENARDY, M., ZALESKI, S., JOSSERAND, C., DRUMRIGHT-CLARKE, M.A., RICHARD, D., CLANET, C. & QUÉRÉ, D. 2003 Pyramidal and toroidal water drops after impact on a solid surface.

SHARMA, V., SZYMUSIAK, M., SHEN, H., NITSCHE, L.C. & LIU, Y. 2012 Formation of polymeric toroidal-spiral particles. *Langmuir* **28** (1), 729–735.

SHUM, H.C., ABATE, A.R., LEE, D., STUDART, A.R., WANG, B., CHEN, C.-H., THIELE, J., SHAH, R.K., KRUMMEL, A. & WEITZ, D.A. 2010 Droplet microfluidics for fabrication of non-spherical particles. *Macromol. Rapid Commun.* **31** (2), 108–118.

SOSTARECZ, M.C. & BELMONTE, A. 2003 Motion and shape of a viscoelastic drop falling through a viscous fluid. *J. Fluid Mech.* **497**, 235–252.

SZYMUSIAK, M., SHARMA, V., NITSCHE, L.C. & LIU, Y. 2012 Interaction of sedimenting drops in a miscible solution–formation of heterogeneous toroidal-spiral particles. *Soft Matt.* **8** (29), 7556–7559.

TEXIER, B.D., PIROIRD, K., QUÉRÉ, D. & CLANET, C. 2013 Inertial collapse of liquid rings. *J. Fluid Mech.* **717**.

ZABARANKIN, M., LAVRENTEVA, O.M. & NIR, A. 2015 Liquid toroidal drop in compressional Stokes flow. *J. Fluid Mech.* **785**, 372–400.

ZABARANKIN, M., SMAGIN, I., LAVRENTEVA, O.M. & NIR, A. 2013 Viscous drop in compressional Stokes flow. *J. Fluid Mech.* **720**, 169–191.